PCCP

ROYAL SOCIETY OF CHEMISTRY

PAPER

View Article Online
View Journal | View Issue

Check for updates

Cite this: *Phys. Chem. Chem. Phys.*, 2020, **22**, 16796

Comparative investigation of the thermal transport properties of Janus SnSSe and SnS_2 monolayers

Gang Liu, *[a] Hui Wang,[a] Zhibin Gao *[b] and Guo-Ling Li[c]

Recently, Janus two-dimensional (2D) materials as a new member of 2D derivatives have been receiving much attention due to their novel properties. In this work, the lattice thermal conductivity κ_L of the Janus SnSSe monolayer is investigated based on first-principles calculations, while that of the SnS_2 monolayer is studied for comparison. It is found the the κ_L values of SnSSe and SnS_2 are 13.3 and 11.0 W m^{-1} K^{-1} at room temperature, and acoustic branches dominate their thermal transport. Weaker phonon anharmonicity in SnSSe leads to a slightly higher κ_L, though it has weaker phonon harmonicity. The smaller Grüneisen parameters of TA and LA phonons lower than 1 THz in SnSSe indicate weaker phonon anharmonicity, resulting in a higher κ_L. Finally, the size effect and boundary effect are also investigated, exhibiting that the κ_L can further decrease at the nanoscale. Our work suggests that Janus SnSSe and SnS_2 have a much lower κ_L compared with conventional transition metal dichalcogenides (TMDs) and are potential competitors in the thermoelectric field.

Received 10th April 2020,
Accepted 23rd June 2020

DOI: 10.1039/d0cp01939a

rsc.li/pccp

Published on 01 July 2020. Downloaded by National University of Singapore on 7/8/2021 7:30:56 AM.

Introduction

The successful exfoliation of graphene has opened up new fields in the study of two-dimensional (2D) materials since 2004.[1] Stimulated by graphene, many other 2D materials have been synthesized experimentally or predicted theoretically, such as hexagonal boron nitride,[2] transition metal chalcogenides (TMDs),[3–6] group-V 2D materials,[7–16] and group-VI 2D materials.[17–22] Among these 2D materials, TMDs attract remarkable attention due to their distinctive physical and chemical properties, such as finite direct band gaps, high on/off ratios (as high as 10^3–10^8), high carrier mobilities and strong optoelectronic responses, as well as their various potential applications.[5,23–27]

In ancient Roman mythology, Janus was the god of gates, time, duality, and doorways, who is characterized by two faces. Recently, as a new member of 2D derivatives, Janus 2D materials have been receiving much attention, since the Janus monolayer MoSSe is synthesized by well-controlled sulfurization of the $MoSe_2$ monolayer, in which the top Se layer is substituted by vaporized sulfur.[28,29] Compared to perfect 2D materials, Janus monolayers with a broken reflection symmetry allow out-of-plane intrinsic electric polarization. Thus, Janus monolayers display many novel properties, such as large Rashba effect, chiral effect, and spatial isolation of charge carriers.[30–35] Furthermore, theoretical investigations show that the thermal transport properties of Janus monolayers are also significantly affected. For instance, the thermal conductivities of MoSSe and PtSSe are suppressed much more compared to those of MoS_2 and PtS_2.[36,37] The thermoelectric performance is measured by using the figure of merit ZT, which is expressed as $ZT = S^2\sigma T/(\kappa_e + \kappa_L)$. Here, $S^2\sigma$ means the power factor, while κ_e and κ_L are the electrical and lattice thermal conductivities. For a semiconductor, κ_e is much smaller than κ_L, and it is concluded that low thermal conductivity leads to high thermoelectric efficiency.

In this work, we systemically investigate the thermal transport properties of Janus SnSSe monolayers, which are constructed based on the synthesized 1T structure of SnS_2/$SnSe_2$.[38,39] The thermal transport properties of the SnS_2 monolayer are also studied, to explore the effect of the Janus structure on thermal transport. Based on first-principles calculations, the lattice thermal conductivity κ_L is obtained by solving the linearized phonon transport Boltzmann equation (BTE). We found that they are 13.3 and 11.0 W m^{-1} K^{-1} at room temperature, while acoustic branches dominate the thermal transport of both the monolayers. Different from other Janus monolayers,[36,37] the two monolayers have κ_L close to each other, showing that the Janus structure does not have a remarkable effect on thermal transport. The harmonic properties, such as phonon spectra, and mechanical properties, Debye temperature, and phonon group velocities, are exhibited.

[a] *School of Physics and Engineering, Henan University of Science and Technology, Luoyang 471023, People's Republic of China. E-mail: liugang8105@gmail.com*
[b] *Department of Physics, National University of Singapore, Singapore 117551, Republic of Singapore. E-mail: zhibin.gao@nus.edu.sg*
[c] *Chemistry and Chemical Engineering Guangdong Laboratory, Shantou 515063, People's Republic of China*

This journal is © the Owner Societies 2020

Published on 01 July 2020. Downloaded by National University of Singapore on 7/8/2021 7:30:56 AM.

To explore the underlying physical mechanisms of the approximately identical κ_L of the two monolayers, anharmonic properties are also investigated, such as relaxation times, the total phase space for three-phonon processes, and Grüneisen parameters. It is found the smaller Grüneisen parameters of TA and LA phonons with low frequency in SnSSe result in a slightly higher κ_L in SnSSe, though it exhibits weaker harmonic properties. Comprehensively, the weaker anharmonic properties enhance the thermal transport in Janus SnSSe, making its κ_L close to that of SnS_2. To study the size and the boundary effect, the cumulative and size-dependent κ_L are also exhibited.

Computational methods

Based on density functional theory (DFT), all the first-principles calculations are performed by using the VASP package.[40–42] Generalized gradient approximations parameterized by Perdew, Burke, and Ernzerhof (PBE) are chosen for exchange–correlation functional.[43] A plane-wave basis set with a kinetic energy cutoff of 500 eV is used. During the structural relaxation, a Monkhorst–Pack[44] k-mesh of $15 \times 15 \times 1$ is used to sample the Brillouin zone (BZ), while the energy and the Hellman–Feynman force convergence thresholds are 10^{-6} eV and 10^{-4} eV Å^{-1}, respectively. A vacuum space of at least 20 Å is maintained along the z direction, which is enough to eliminate the interactions between the adjacent layers.

Due to the isotropic in-plane structure of the SnSSe monolayer, the in-plane κ_L is also isotropic and can be calculated as:

$$\kappa_L = \frac{1}{V}\sum_{\lambda} C_\lambda v_{\lambda\alpha}{}^2 \tau_{\lambda\alpha}, \quad (1)$$

where V is the cell volume and λ is the phonon mode which comprises both the wave vector index $\boldsymbol{q}$ and the phonon branch index j. Furthermore, C_λ is the heat capacity in each mode; $v_{\lambda\alpha}$ is the group velocity of the phonon along the α direction, with the mode index λ; and $\tau_{\lambda\alpha}$ is the relaxation time of the phonon with λ mode along the same direction. Based on eqn (1), κ_L is determined based on both harmonic and anharmonic properties. The harmonic interatomic force constants (IFCs) were calculated using a $6 \times 6 \times 1$ supercell and a $2 \times 2 \times 1$ k-mesh within a finite displacement scheme, as implemented in the open-source software package PHONOPY.[45] Then the phonon dispersion relation can be obtained using the harmonic IFCs. The anharmonic IFCs were calculated using ShengBTE code,[46] considering up to the ninth-nearest neighbor. After careful parameter testing, the converged κ_L was obtained with a $\mathbf{q}$-mesh of $201 \times 201 \times 1$, and a scale broadening parameter of 0.1 was used for Gaussian smearing. Note that an effective thickness should be defined to calculate the thermal properties for 2D materials. For SnSSe, the thickness of 6.78 Å was considered as the summation of the buckling height h and the van der Waals radii of the S and Se atoms.[47–49] And for SnS_2 the thickness was 6.55 Å under the same definition.

Results and discussion

The optimized structure of the Janus SnSSe monolayer is shown in Fig. 1(a), while that of the SnS_2 monolayer is exhibited in Fig. 1(b). It is found that they share a similar structure; nevertheless, in SnSSe the Sn atom layer is sandwiched between the S and Se atom layers, with a broken reflection symmetry along the out-of-plane direction. Thus, its structure belongs to the $P3m1$ (156) symmetry group, whose symmetry is lower than $P\bar{3}m1$ (164) for SnS_2. Note that they belong to the same trigonal crystal system but with different subgroups due to the broken reflection symmetry, which could induce piezoelectric properties in Janus materials, such as SnSSe. The lattice constant a and the buckling height h are 3.78 and 3.08 Å for SnSSe, while the corresponding values are 3.70 and 2.96 Å for SnS_2. These results are in good agreement with those in previous researches.[50,51] In general, a larger lattice constant implies weaker interatomic bonding in SnSSe.

Usually, we can estimate κ_L based on the Slack model:[52]

$$\kappa_L \sim \frac{a^4 \rho \omega_D{}^3}{\gamma^2 T}, \quad (2)$$

where a^3, ρ, ω_D and T are the average volume occupied by one atom of the crystal, the density, the Debye frequency, and the

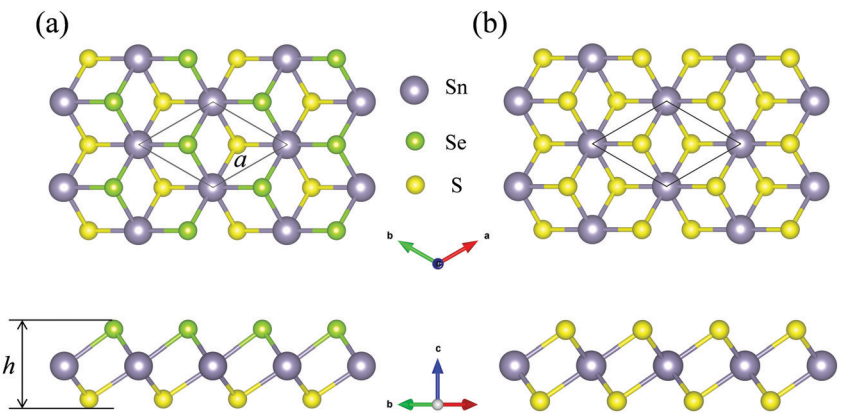

Fig. 1 (a) Structure of the Janus SnSSe monolayer and (b) the structure of the SnS_2 monolayer. Both top and side views are exhibited. The primitive cells are marked in solid lines.

Published on 01 July 2020. Downloaded by National University of Singapore on 7/8/2021 7:30:56 AM.

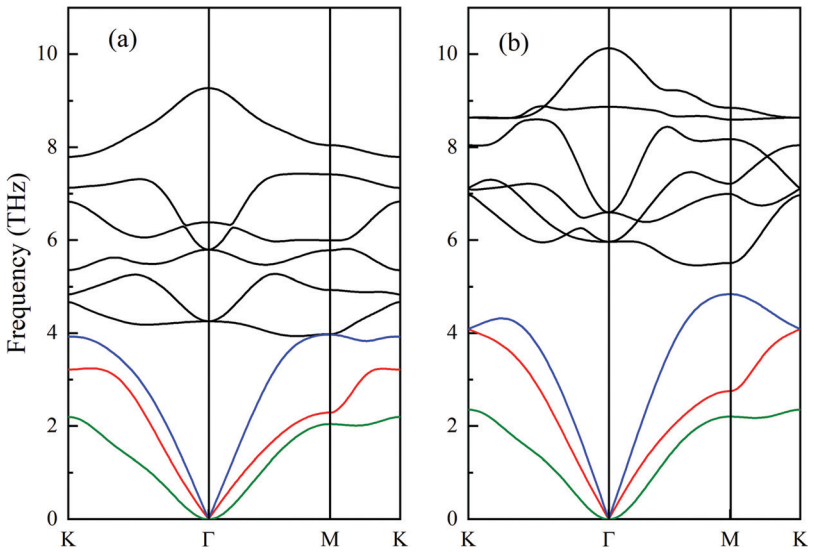

Fig. 2 Phonon dispersions for SnSSe (a) and SnS_2 (b) monolayers. Three acoustic phonon branches, which correspond to an out-of-plane (ZA) mode, an in-plane transverse (TA) mode, and an in-plane longitudinal (LA) mode, are marked in green, red and blue colors.

absolute temperature. The Grüneisen parameter γ is expressed as $\gamma = -\frac{\mathrm{d}\ln\omega}{\mathrm{d}\ln V}$, exhibiting phonon anharmonicity. This indicates that both stronger harmonicity and weaker anharmonicity lead to a higher κ_L. The phonon dispersions for the monolayers SnSSe and SnS_2 are displayed in Fig. 2, which show the phonon harmonicity of the materials. There is no imaginary frequency indicating the dynamic stability of the two structures. For both the monolayers, there are 9 branches as each primitive cell possesses 3 atoms. On the whole, the phonon dispersions are very similar to each other. However, the phonon frequencies for each branch are lower in SnSSe, resulting from the heavier average atomic mass M, as listed in Table 1. In general, the average phonon frequency is inversely proportional to the average atomic mass, the same as the maximum vibrational frequencies. Furthermore, there is no phonon gap in Janus SnSSe, whereas it appears in the phonon dispersion of SnS_2. It should be noted that the phonon gap generally can suppress phonon scattering, and hence enhance thermal transport.[53]

The 2D elastic constants and Young's moduli are calculated, as shown in Table 1. It should be noted that the calculated elastic constants satisfy the Born criteria of mechanical stability.[54] The 2D Young's modulus E is calculated based on elastic constants with the following expression: $E = (C_{11}^2 - C_{12}^2)/C_{11}$.[55] It is found that the 2D elastic constants and Young's moduli for SnSSe are slightly smaller than those for SnS_2, due to the larger lattice constant and weaker interatomic bonding in SnSSe. Their E are close to those of α-selenene and β-arsenene,[56] but smaller than those of blue phosphorene, the MoS_2 monolayer, and graphene.[56–58] Furthermore, our results are in good agreement with those in previous work.[50]

Table 1 2D elastic constants and Young's moduli (in N m^{-1}), Debye temperature (in K), average atomic mass M (in amu), and group velocities of the three acoustic phonons (in km s^{-1}) around the Γ point

	C_{11}	C_{12}	C_{66}	E	v_{ZA}	v_{TA}	v_{LA}	M	θ_D
SnSSe	63.8	15.9	23.9	59.8	0.263	2.521	3.992	76.6	190
SnS_2	69.7	17.0	26.3	65.6	0.139	3.052	4.788	60.9	233

The group velocity is denoted as $\vec{v} = \mathrm{d}\omega/\mathrm{d}\vec{q}$, while the Debye temperature θ_D is denoted as $\theta_D = \hbar\omega_D/k_B$, where ω_D can be considered as the maximum acoustic phonon frequency.[21,48,59] The group velocities of the acoustic phonons around the Γ point and Debye temperature θ_D for SnSSe and SnS_2 are also listed in Table 1. The phonon group velocities of TA and LA modes for SnSSe are smaller than that for SnS_2, whereas the phonon group velocity of ZA phonons is larger in SnSSe. θ_D is smaller in SnSSe than in SnS_2, to the benefit of lower κ_L in SnSSe based on eqn (2).

The intrinsic κ_L of the monolayers SnSSe and SnS_2 are calculated by ShengBTE with an iterative scheme,[46] as displayed in Fig. 3. The κ_L of the monolayer SnSSe is higher than that of SnS_2 in the whole temperature range. For instance, the values are 13.3 and 11.0 W m^{-1} K^{-1} at 300 K, which are close to each other. The intrinsic κ_L for both the monolayers show an inverse dependence on temperature T, implying the dominant Umklapp process of phonon–phonon scattering in the thermal transport. It is found that the κ_L of the monolayer SnS_2 is slightly lower than the in-plane κ_L of 12.1 W m^{-1} K^{-1} for bulk SnS_2,[60] which does not follow the unique trend of 2D SnS_2 that κ_L decreases with decreasing thickness.[61] The reason for a slightly higher κ_L of the SnSSe monolayer which has lower harmonic properties than SnS_2 will be discussed later. The values are much smaller than that of MoS_2 with 131 W m^{-1} K^{-1},[62] implying potential competitors in the thermoelectric field. For instance, previous work shows an excellent power factor of about 65 μW cm^{-1} K^{-2} with a doping level of 0.0248 at 700 K in the SnSSe monolayer.[50] Considering that the lattice thermal conductivity is 5.0 W m^{-1} K^{-1} at the same temperature, SnSSe possesses a high ZT of about 0.9.

 This journal is © the Owner Societies 2020

Published on 01 July 2020. Downloaded by National University of Singapore on 7/8/2021 7:30:56 AM.

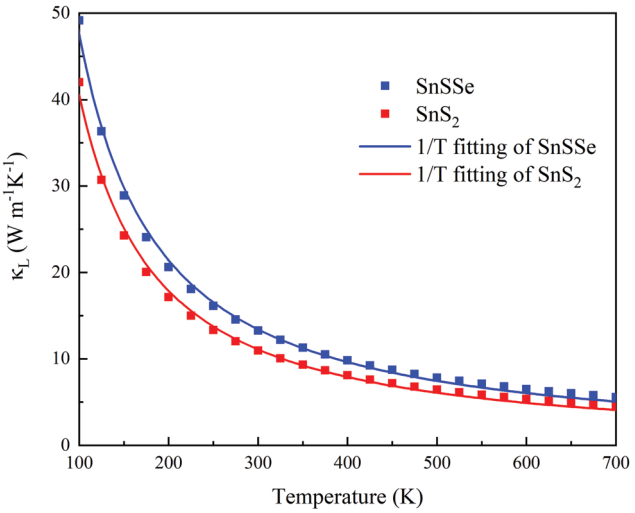

Fig. 3 Temperature-dependent κ_L of the monolayers SnSSe and SnS_2. $1/T$ fittings are shown in solid lines.

Furthermore, we also use thermal sheet conductance ("2D thermal conductivity") with the unit W K^{-1} as it is more meaningful and physical for 2D materials.[63,64] Then we obtain values of 8.99 and 7.17 nW K^{-1} for the SnSSe and SnS_2 monolayers at 300 K, respectively. For comparison, it was reported that the thermal sheet conductances are 57.04, 34.25, and 28.44 nW K^{-1} for the MoS_2, MoSSe, and $MoSe_2$ monolayers, respectively.[36] It can be seen that Janus SnSSe possesses much lower thermal sheet conductance than Janus MoSSe.

It is found that the acoustic phonons contribute most to the total κ_L. For SnSSe, we found that ZA, TA and LA modes contribute 27.1%, 35.7% and 35.3% to the total κ_L at room temperature, while all the optical branches contribute 1.9% only. For SnS_2, the normalized contributions of ZA, TA, and LA modes are 33.5%, 30.7%, and 31.3%, respectively, while the one of all the optical modes is 4.5%. It is found that the contribution of ZA mode is lower in SnSSe than in SnS_2. Note that the contribution of the ZA mode is much lower than that in graphene (about 75%), and it is believed that the domination comes from the unique symmetry of flat graphene along its *c*-axis.[65,66] There is a symmetry selection rule in flat graphene that only an even number of ZA modes can be involved in scattering processes. This rule originates from the reflection symmetry about the *c*-axis in the structure. The thermal resistance originates from the anharmonic phonon scattering. Due to the selection rule, the ZA mode contributes mainly to the total thermal conductivity in graphene. However, the lattice does not have a reflection symmetry along the *c*-axis in Janus SnSSe and SnS_2. As a result, the selection rule is broken and the contribution of the ZA mode in the thermal transport of the two materials is much lower than that in graphene.

To further understand the underlying physical mechanisms of κ_L in these two monolayers, we investigate the phonon group velocity and the relaxation time, as shown in Fig. 4. On the

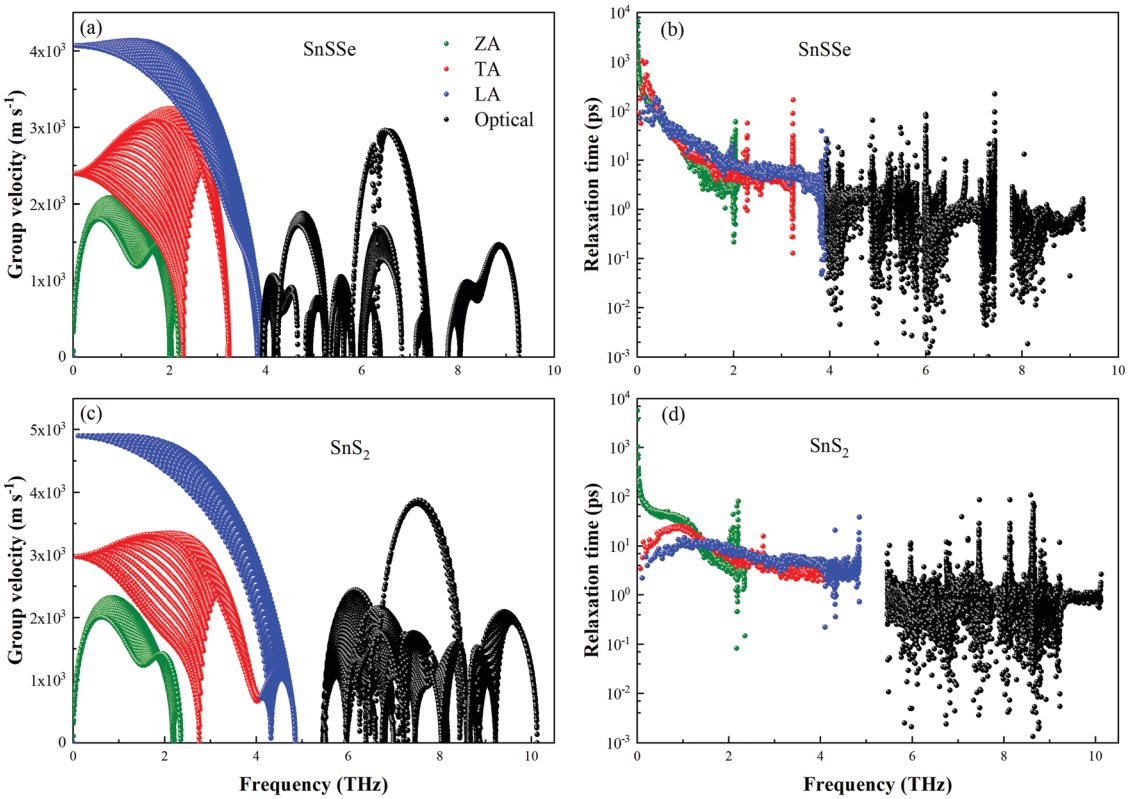

Fig. 4 Phonon group velocities and relaxation times of the two monolayers at room temperature; (a) and (b) display the group velocity and relaxation time of SnSSe, while (c) and (d) show the group velocity and relaxation time of SnS_2.

Published on 01 July 2020. Downloaded by National University of Singapore on 7/8/2021 7:30:56 AM.

whole, the phonon group velocities of the two monolayers are similar, whereas those of SnSSe are lower. The range of group velocity is from 0 to 4000 m s^{-1} for SnSSe, while it is from 0 to 5000 m s^{-1} for SnS_2. Furthermore, compared to Janus SnSSe, the phonon group velocity of phonons with a low frequency is as high as 5500 m s^{-1} in the MoSSe monolayer, leading to a higher thermal conductivity in MoSSe.[36] This also confirms that heavier M leads to weaker phonon harmonicity in SnSSe, as mentioned previously. The phonon group velocities of acoustic modes are higher than those of optical modes because of the relative flatness of optical modes.

The relaxation time is inversely related to the strength of anharmonic interaction, which is in the range of 10^{-3} to 10^{4} ps for both the monolayers as displayed in Fig. 4(b) and (d). However, there are remarkable differences between TA and LA phonons with a low frequency between the two monolayers. The relaxation times of TA and LA phonons below 1 THz for SnSSe are one order higher than those for SnS_2. Based on eqn (1), the κ_L is mainly determined based on the group velocity and the relaxation time. It is mentioned above that TA and LA modes contribute more than 60% to the κ_L in both the monolayers. Therefore, the much smaller relaxation time of TA and LA phonons below 1 THz determines the smaller κ_L in SnS_2, though SnS_2 possesses stronger phonon harmonic properties. Furthermore, the relaxation times of many phonons show a large decrease near 4 THz in SnSSe, which is the cross-region of acoustic and optical branches. However, there is no such situation near the acoustic-optical gap (5 THz) in SnS_2, confirming the effect of enhancing the thermal transport for the acoustic-optical gap.[53]

The intrinsic phonon scattering rate $1/\tau_\lambda^0$ (inversion of the relaxation time) determined by three-phonon transition probabilities can be expressed in the following equations:

$$\frac{1}{\tau_\lambda^0} = \frac{1}{N}\left(\sum_{\lambda' \lambda''} \Gamma_{\lambda\lambda'\lambda''}^{+} + \sum_{\lambda' \lambda''} \frac{1}{2}\Gamma_{\lambda\lambda'\lambda''}^{-}\right), \quad (3)$$

$$\Gamma_{\lambda\lambda'\lambda''}^{+} = \frac{\hbar\pi}{4}\frac{(f_0' - f_0'')}{\omega_\lambda \omega_{\lambda'} \omega_{\lambda''}} |V_{\lambda\lambda'\lambda''}^{+}|^2 \delta(\omega_\lambda + \omega_{\lambda'} - \omega_{\lambda''}), \quad (4)$$

$$\Gamma_{\lambda\lambda'\lambda''}^{-} = \frac{\hbar\pi}{4}\frac{(f_0' + f_0'' + 1)}{\omega_\lambda \omega_{\lambda'} \omega_{\lambda''}} |V_{\lambda\lambda'\lambda''}^{-}|^2 \delta(\omega_\lambda - \omega_{\lambda'} - \omega_{\lambda''}), \quad (5)$$

where f_0 means Bose–Einstein statistics of the phonon mode λ, $\Gamma_{\lambda\lambda'\lambda''}^{+}$ and $\Gamma_{\lambda\lambda'\lambda''}^{-}$ stand for the absorption and emission processes, and N is the number of $\boldsymbol{q}$ points in BZ.[46] Furthermore, $V_{\lambda\lambda'\lambda''}^{\pm}$ means the scattering matrix elements, which are proportional to anharmonic IFCs.[46,48] As mentioned previously, the Grüneisen parameter γ indicates the anharmonicity of the materials, thus γ is proportional to $V_{\lambda\lambda'\lambda''}^{\pm}$ and the scattering rate. It is also in agreement with the Slack model in eqn (2), which implies that κ_L is inversely proportional to γ. Based on

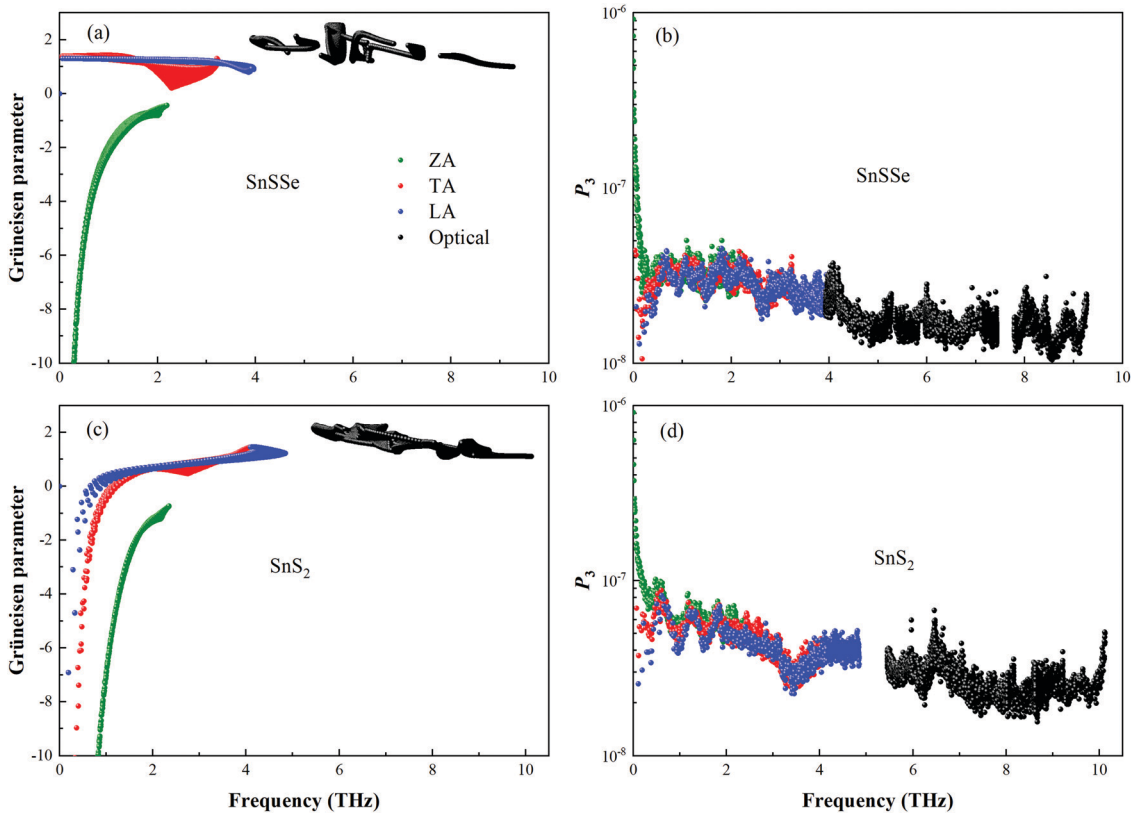

Fig. 5 Grüneisen parameter γ and P_3 for the monolayers SnSSe and SnS_2; (a) and (b) show γ and P_3 of SnSSe, while (c) and (d) display those quantities of SnS_2.

 This journal is © the Owner Societies 2020

Published on 01 July 2020. Downloaded by National University of Singapore on 7/8/2021 7:30:56 AM.

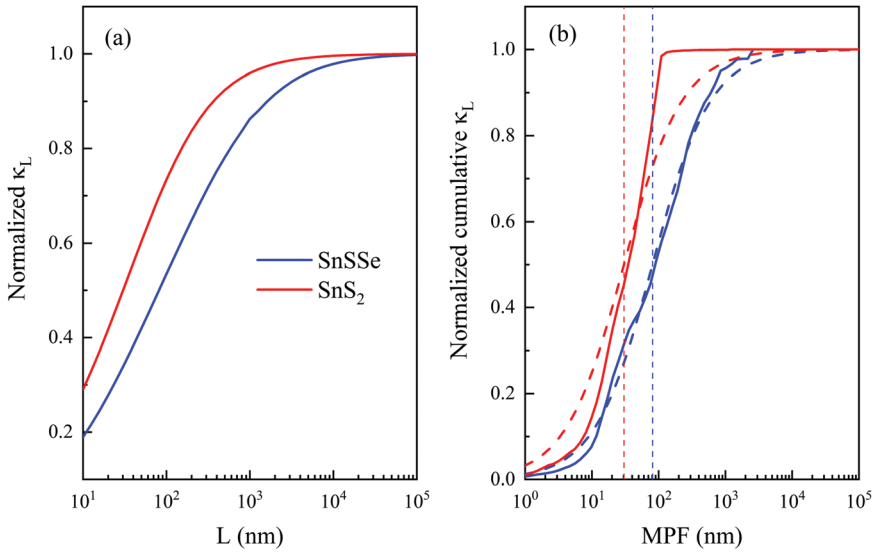

Fig. 6 (a) Normalized κ_L as a function of the sample size L at 300 K. (b) Normalized cumulative κ_L as a function of the phonon MPF of the monolayers SnSSe and SnS_2 at 300 K. The dashed lines in (b) indicate the fitting data. The vertical lines indicate the position of l_0 for the two monolayers.

eqn (3)–(5), it is also found that the scattering rate is proportional to the number of Dirac delta distributions, which can be denoted by the volume of the scattering phase space P_3 for three-phonon processes.[46] We have calculated γ and P_3, as exhibited in Fig. 5. For P_3, a significant increase near 4 THz in SnSSe can be seen, while there is a decrease near 5 THz in SnS_2. This indicates the suppression effect on scattering for the acoustic-optical gap, thus the acoustic-optical gap can enhance the relaxation time as displayed in Fig. 4. However, it cannot lead to lower κ_L in Janus SnSSe, as most of the contributions to κ_L come from phonons with a low frequency. We found that there are obvious distinctions for γ of TA and LA phonons with low frequency. Specifically, γ is around 1.6 for TA and LA phonons with a frequency lower than 1 THz in SnSSe, while it shows negative values with a very large absolute value in SnS_2. Therefore, γ leads to a discrepancy of the relaxation time of these low-frequency phonons in two monolayers, and finally suppresses the κ_L of SnS_2, though it possesses higher phonon harmonicity than SnSSe, such as group velocity, Young's modulus, and Debye temperature. In conclusion, the much weaker phonon anharmonicity in SnSSe compensates the weaker harmonicity, and even leads to a slightly higher κ_L.

In practical applications, all materials have a finite size which can suppress κ_L significantly through boundary scattering of different sample sizes, especially at the nanoscale. Here, an empirical formula is used to describe the boundary scattering, expressed as: $\frac{1}{\tau_\lambda^b} = \frac{v_\lambda}{L}$, where L means the size of the material.[67,68] The calculated results are shown in Fig. 6(a). The κ_L of the two monolayers reduces following an exponential function of increasing L due to the strong boundary effect, which has been experimentally verified in suspended graphene.[69] It is found the the κ_L of the Janus SnSSe monolayer decreases more quickly than that of the SnS_2 monolayer with diminishing size. For instance, the normalized κ_L of the SnSSe monolayer is 0.53 at a size of 100 nm, while that of the SnS_2 monolayer is 0.73. When the L is 1000 nm, the data are 0.86 and 0.96, respectively.

To estimate the size effect, we also evaluate the normalized cumulative κ_L with respect to the phonon mean free paths (MFPs) for both the monolayers, as shown in Fig. 6(b). The phonon MFPs which contribute mainly to κ_L span from 1 to 1000 nm for SnSSe, whereas the range is from 1 to 100 nm for SnS_2, much narrower than the former. This indicates that phonons with a low frequency contribute more to κ_L in SnS_2 than in SnSSe. In order to obtain the characteristic length, we introduce a single parametric function:[46]

$$\kappa_L(l \le l_{max}) = \frac{\kappa_{max}}{1 + l_0/l_{max}}, \quad (6)$$

where l_{max} and κ_{max} are the maximum MFP and the ultimate cumulative lattice thermal conductivity. l_0 is the only parameter to be determined, and can be regarded as the representative MFP. It is found that l_0 values are 80.9 and 30.2 nm for the SnSSe and SnS_2 monolayers, respectively, corresponding to the positions of 50% of the total κ_L. This is in good agreement with the curves shown in Fig. 6(a), indicating a much weaker size effect in the phonon transport of the nanoscale SnSSe than SnS_2. It can be expected that the κ_L will significantly decrease when the size is of the order of 100 nm. This information is very useful for the thermal management design of micro-/nano-electronic devices based on these monolayers.

Conclusion

In summary, the lattice thermal conductivities κ_L of Janus SnSSe and SnS_2 monolayers are investigated based on first-principles calculations. The κ_L values of SnSSe and SnS_2 are 13.3 and 11.0 W m^{-1} K^{-1} at room temperature, which are close to each other. Acoustic branches dominate the thermal transport of the two monolayers. The harmonic and anharmonic

Published on 01 July 2020. Downloaded by National University of Singapore on 7/8/2021 7:30:56 AM.

phonon properties together determine the κ_L of the materials, thus they are further investigated. It is found that the SnS_2 monolayer possesses stronger harmonic properties than the Janus SnSSe monolayer, such as higher elastic constants, Young's modulus, phonon group velocity and θ_D. However, the SnSSe monolayer has a slightly higher κ_L than SnS_2 due to the weaker anharmonic scattering than the former. Smaller Grüneisen parameters of LA and TA phonons within 1 THz are found in SnSSe, exhibiting lower anharmonicity of these phonons. And this finally leads to higher relaxation times and κ_L in the Janus SnSSe monolayer. At last, the size and boundary effects are studied by cumulative κ_L and size-dependent κ_L, respectively. This provides important information for the future design of micro-/nano-devices. It can be expected that our work may contribute to the understanding of the thermal transport of 2D materials, as well as the practical applications of SnSSe and SnS_2 monolayers.

Conflicts of interest

There are no conflicts to declare.

Acknowledgements

This work was supported by the National Natural Science Foundation of China (No. 11974100). Z. Gao acknowledges financial support from MOE Tier 1 funding of Singapore (Grant No. R-144-000-402-114).

References

1 K. S. Novoselov, A. K. Geim, S. V. Morozov, D. Jiang, Y. Zhang, S. V. Dubonos, I. V. Grigorieva and A. A. Firsov, *Science*, 2004, **306**, 666.
2 S. Hu, M. Lozada-Hidalgo, F. C. Wang, A. Mishchenko, F. Schedin, R. R. Nair, E. W. Hill, D. W. Boukhvalov, M. I. Katsnelson and R. A. Dryfe, *et al.*, *Nature*, 2014, **516**, 227.
3 C. Ataca, H. Şahin and S. Ciraci, *J. Phys. Chem. C*, 2012, **116**, 8983.
4 J. N. Coleman, M. Lotya, A. O'Neill, S. D. Bergin, P. J. King, U. Khan, K. Young, A. Gaucher, S. De and R. J. Smith, *et al.*, *Science*, 2011, **331**, 568.
5 K. F. Mak, C. Lee, J. Hone, J. Shan and T. F. Heinz, *Phys. Rev. Lett.*, 2010, **105**, 136805.
6 Y. Zhan, Z. Liu, S. Najmaei, P. M. Ajayan and J. J. S. Lou, *Small*, 2012, **8**, 966.
7 Z. Zhu and D. Tomanek, *Phys. Rev. Lett.*, 2014, **112**, 176802.
8 S. Zhang, Z. Yan, Y. Li, Z. Chen and H. Zeng, *Angew. Chem., Int. Ed.*, 2015, **54**, 3112.
9 G. Wang, R. Pandey and S. P. Karna, *ACS Appl. Mater. Interfaces*, 2015, **7**, 11490.
10 Z. Zhu, J. Guan and D. Tománek, *Phys. Rev. B: Condens. Matter Mater. Phys.*, 2015, **91**, 161404.
11 C. Kamal and M. Ezawa, *Phys. Rev. B: Condens. Matter Mater. Phys.*, 2015, **91**, 085423.
12 O. Ü. Aktürk, V. O. Özçelik and S. Ciraci, *Phys. Rev. B: Condens. Matter Mater. Phys.*, 2015, **91**, 235446.
13 S. Zhang, M. Xie, F. Li, Z. Yan, Y. Li, E. Kan, W. Liu, Z. Chen and H. Zeng, *Angew. Chem., Int. Ed.*, 2016, **55**, 1666.
14 H. Liu, A. T. Neal, Z. Zhu, Z. Luo, X. Xu, D. Tomanek and P. D. Ye, *ACS Nano*, 2014, **8**, 4033.
15 V. Tran, R. Soklaski, Y. Liang and L. Yang, *Phys. Rev. B: Condens. Matter Mater. Phys.*, 2014, **89**, 235319.
16 L. Li, Y. Yu, G. J. Ye, Q. Ge, X. Ou, H. Wu, D. Feng, X. H. Chen and Y. Zhang, *Nat. Nanotechnol.*, 2014, **9**, 372.
17 Z. Zhu, X. Cai, S. Yi, J. Chen, Y. Dai, C. Niu, Z. Guo, M. Xie, F. Liu and J. H. Cho, *et al.*, *Phys. Rev. Lett.*, 2017, **119**, 106101.
18 J. Chen, Y. Dai, Y. Ma, X. Dai, W. Ho and M. Xie, *Nanoscale*, 2017, **9**, 15945.
19 J. Qin, G. Qiu, J. Jian, H. Zhou, L. Yang, A. Charnas, D. Y. Zemlyanov, C. Y. Xu, X. Xu and W. Wu, *et al.*, *ACS Nano*, 2017, **11**, 10222.
20 G. Liu, Z. Gao and J. Ren, *Phys. Rev. B: Condens. Matter Mater. Phys.*, 2019, **99**, 195436.
21 Z. Gao, G. Liu and J. Ren, *ACS Appl. Mater. Interfaces*, 2018, **10**, 40702.
22 S. Sharma, N. Singh and U. Schwingenschlögl, *ACS Appl. Mater. Interfaces*, 2018, **1**, 1950.
23 B. Radisavljevic, A. Radenovic, J. Brivio, V. Giacometti and A. Kis, *Nat. Nanotechnol.*, 2011, **6**, 147.
24 S.-W. Min, H. S. Lee, H. J. Choi, M. K. Park, T. Nam, H. Kim, S. Ryu and S. Im, *Nanoscale*, 2013, **5**, 548.
25 M. Bernardi, M. Palummo and J. C. Grossman, *Nano Lett.*, 2013, **13**, 3664.
26 W. Zhang, Z. Huang, W. Zhang and Y. J. N. R. Li, *Nano Res.*, 2014, **7**, 1731.
27 Z. Hui, W. Xu, X. Li, P. Guo, Y. Zhang and J. Liu, *Nanoscale*, 2019, **11**, 6045.
28 A.-Y. Lu, H. Zhu, J. Xiao, C.-P. Chuu, Y. Han, M.-H. Chiu, C.-C. Cheng, C.-W. Yang, K.-H. Wei and Y. Yang, *et al.*, *Nat. Nanotechnol.*, 2017, **12**, 744.
29 J. Zhang, S. Jia, I. Kholmanov, L. Dong, D. Er, W. Chen, H. Guo, Z. Jin, V. B. Shenoy and L. Shi, *et al.*, *ACS Nano*, 2017, **11**, 8192.
30 Q.-F. Yao, J. Cai, W.-Y. Tong, S.-J. Gong, J.-Q. Wang, X. Wan, C.-G. Duan and J. H. Chu, *Phys. Rev. B: Condens. Matter Mater. Phys.*, 2017, **95**, 165401.
31 F. Li, W. Wei, P. Zhao, B. Huang and Y. Dai, *J. Phys. Chem. Lett.*, 2017, **8**, 5959.
32 W.-J. Yin, B. Wen, G.-Z. Nie, X.-L. Wei and L.-M. Liu, *J. Mater. Chem. C*, 2018, **6**, 1693.
33 T. Hu, F. Jia, G. Zhao, J. Wu, A. Stroppa and W. Ren, *Phys. Rev. B: Condens. Matter Mater. Phys.*, 2018, **97**, 235404.
34 J. Liang, W. Wang, H. Du, A. Hallal, K. Garcia, M. Chshiev, A. Fert and H. Yang, *Phys. Rev. B: Condens. Matter Mater. Phys.*, 2020, **101**, 184401.
35 G. Radovsky, R. Popovitz-Biro and R. Tenne, *Chem. Mater.*, 2012, **24**, 3004.
36 S. D. Guo, *Phys. Chem. Chem. Phys.*, 2018, **20**, 7236.
37 W.-L. Tao, Y. Mu, C.-E. Hu, Y. Cheng and G.-F. Ji, *Philos. Mag.*, 2019, **99**, 1025.

 This journal is © the Owner Societies 2020

Published on 01 July 2020. Downloaded by National University of Singapore on 7/8/2021 7:30:56 AM.

38 X. Zhou, Q. Zhang, L. Gan, H. Li and T. Zhai, *Adv. Funct. Mater.*, 2016, **26**, 4405.
39 X. Zhou, L. Gan, W. Tian, Q. Zhang, S. Jin, H. Li, Y. Bando, D. Golberg and T. Zhai, *Adv. Mater.*, 2015, **27**, 8035.
40 G. Kresse and J. Hafner, *Phys. Rev. B: Condens. Matter Mater. Phys.*, 1993, **47**, 558.
41 G. Kresse and J. Furthmüller, *Comput. Mater. Sci.*, 1996, **6**, 15.
42 G. Kresse and J. Furthmüller, *Phys. Rev. B: Condens. Matter Mater. Phys.*, 1996, **54**, 11169.
43 J. P. Perdew, K. Burke and M. Ernzerhof, *Phys. Rev. Lett.*, 1996, **77**, 3865.
44 H. J. Monkhorst and J. D. Pack, *Phys. Rev. B: Solid State*, 1976, **13**, 5188.
45 A. Togo, F. Oba and I. Tanaka, *Phys. Rev. B: Condens. Matter Mater. Phys.*, 2008, **78**, 134106.
46 W. Li, J. Carrete, N. A. Katcho and N. Mingo, *Comput. Phys. Commun.*, 2014, **185**, 1747.
47 M. Hu, X. Zhang and D. Poulikakos, *Phys. Rev. B: Condens. Matter Mater. Phys.*, 2013, **87**, 195417.
48 Z. Gao, Z. Zhang, G. Liu and J. S. Wang, *Phys. Chem. Chem. Phys.*, 2019, **21**, 26033.
49 G. Liu, H. Wang, Y. Gao, J. Zhou and H. Wang, *Phys. Chem. Chem. Phys.*, 2017, **19**, 2843.
50 S. D. Guo, X. S. Guo, R. Y. Han and Y. Deng, *Phys. Chem. Chem. Phys.*, 2019, **21**, 24620.
51 A. Shafique, A. Samad and Y. H. Shin, *Phys. Chem. Chem. Phys.*, 2017, **19**, 20677.
52 G. A. Slack, *J. Phys. Chem. Solids*, 1973, **34**, 321.
53 L. Lindsay, D. A. Broido and T. L. Reinecke, *Phys. Rev. Lett.*, 2013, **111**, 025901.
54 R. C. Andrew, R. E. Mapasha, A. M. Ukpong and N. Chetty, *Phys. Rev. B: Condens. Matter Mater. Phys.*, 2012, **85**, 125428.
55 Q. Wei and X. Peng, *Appl. Phys. Lett.*, 2014, **104**, 251915.
56 G. Liu, Z. Gao and J. Zhou, *Phys. E*, 2019, **112**, 59.
57 F. Liu, P. Ming and J. Li, *Phys. Rev. B: Condens. Matter Mater. Phys.*, 2007, **76**, 064120.
58 T. Li, *Phys. Rev. B: Condens. Matter Mater. Phys.*, 2012, **85**, 235407.
59 L.-D. Zhao, S.-H. Lo, Y. Zhang, H. Sun, G. Tan, C. Uher, C. Wolverton, V. P. Dravid and M. G. Kanatzidis, *Nature*, 2014, **508**, 373.
60 H. Wang, Y. Gao and G. Liu, *RSC Adv.*, 2017, **7**, 8098.
61 M. J. Lee, J. H. Ahn, J. H. Sung, H. Heo, S. G. Jeon, W. Lee, J. Y. Song, K. H. Hong, B. Choi and S. H. Lee, *et al.*, *Nat. Commun.*, 2016, **7**, 12011.
62 A. N. Gandi and U. Schwingenschlögl, *EPL*, 2016, **113**, 36002.
63 X. Wu, V. Varshney, J. Lee, Y. Pang, A. K. Roy and T. Luo, *Chem. Phys. Lett.*, 2017, **669**, 233.
64 Z. Gao, F. Tao and J. Ren, *Nanoscale*, 2018, **10**, 12997.
65 L. Lindsay, D. A. Broido and N. Mingo, *Phys. Rev. B: Condens. Matter Mater. Phys.*, 2010, **82**, 115427.
66 L. Lindsay, W. Li, J. Carrete, N. Mingo, D. A. Broido and T. L. Reinecke, *Phys. Rev. B: Condens. Matter Mater. Phys.*, 2014, **89**, 155426.
67 A. A. Balandin, S. Ghosh, W. Bao, I. Calizo, D. Teweldebrhan, F. Miao and C. N. Lau, *Nano Lett.*, 2008, **8**, 902.
68 D. L. Nika, E. P. Pokatilov, A. S. Askerov and A. A. Balandin, *Phys. Rev. B: Condens. Matter Mater. Phys.*, 2009, **79**, 155413.
69 X. Xu, L. F. C. Pereira, Y. Wang, J. Wu, K. Zhang, X. Zhao, S. Bae, C. Tinh Bui, R. Xie and J. T. L. Thong, *et al.*, *Nat. Commun.*, 2014, **5**, 3689.